Research Square

Preprints are preliminary reports that have not undergone peer review.
They should not be considered conclusive, used to inform clinical practice,
or referenced by the media as validated information.

Assessment of Spatio-temporal urban heat island dynamics in Bolgatanga municipality, Ghana using multitemporal Landsat imagery

Bumbas Azeez
Asante Gold Bebiani Limited
Joan A. Atulley
jaakandi@utas.edu.gh
C.K. Tedam University of Technology and Applied Sciences
Ramson Kabenla
C.K. Tedam University of Technology and Applied Sciences
Steve Ampofo
C.K. Tedam University of Technology and Applied Sciences

Research Article

Keywords: Urban Heat Island, Spatio Temporal, Temperature, Ghana

Posted Date: June 30th, 2026

DOI: https://doi.org/10.21203/rs.3.rs-9857954/v1

License: This work is licensed under a Creative Commons Attribution 4.0 International License.
Read Full License

Additional Declarations: No competing interests reported.

Assessment of Spatio-temporal urban heat island dynamics in Bolgatanga municipality, Ghana using multitemporal Landsat imagery

Bumbas Azeez[a], Joan A. Atulley[b*], Ramson Kabenla[b], Steve Ampofo[b]

a. Department of Environment, Asante Gold Bebiani Limited, Bibiani, Ghana

b. Department of Environmental Science, University of Technology and Applied Sciences (UTAS), Navrongo, Ghana.

Corresponding author: Joan A. Atulley

Email: jaakandi@utas.edu.gh

Abstract

Urban Heat Island (UHI) marked by extreme heat in developed regions relative to neighboring villages, stands out as a key sign of human induced climate change. This research presents the space-time changing aspects of UHI within the Bolgatanga municipality, Upper East Region, Ghana, leveraging multi-temporal Landsat imagery and meteorological dataset from 2007, 2014 and 2021. Temperature of land surface was acquired using the mono-window algorithm. The method brought together atmospheric transmittance, surface emissivity, and ambient temperature. The findings reveal a progressive intensification of UHI effects with the highest LST appreciation from 33.66˚C in 2007 to 42.46 ˚C in 2021. Spatial analysis shows that built-up and bare land areas show significantly higher thermal signatures compared to vegetation and water areas. The spread of paved surfaces, vegetation cover removal, and weak land use choices are the primary causes of thermal anomalies amplification. This research underscores the application of earth observation techniques in quantifying city thermal anomalies and provides useful findings for climate resilient urban development in rapidly changing sub-Saharan cities.

Key words; Urban Heat Island, Spatio Temporal, Temperature, Ghana

1.0 Introduction

Global urbanization has escalated with the fast pace of technological progress, leading to growing concern over the city-induced warming phenomenon. This phenomenon, marked by warmer temperatures in cities as opposed to their neighboring hinterlands,

has become a focal point of scientific research due to its implications for urban thermal comfort and broader climate dynamics (Nuruzzaman, 2015).

Traditionally, UHI assessments have used Land surface temperature (LST) and local meteorological stations data (Addas et al., 2020). However, ground-based measurement often provides limited spatial coverage and fails to capture the varied thermal characteristics across a complex urban environment, particularly in areas where meteorological stations are sparse (Zhao et al., 2025). With the onboarding of detailed-resolution satellites for observing the Earth, remote sensing has since the 1960s become a pivotal tool for UHI analysis, offering superior spatial resolution and broader geographical coverage (Liu and Zhang, 2011). Satellite-driven LST enable consistent, large-scale monitoring of urban thermal anomalies, making it particularly valuable for data scarce regions such as northern Ghana (Dos Santos et al., 2017). Gui et al., (2019) claim that rapid urbanization and population growth in Wuhan have significantly intensified the UHI effect by transforming natural landscape into built environment, which reduces vegetation cover and alters surface thermal properties. Using Landsat and MODIS Data from 1989 to 2017, the study demonstrates that increased impervious surfaces and diminished vegetation lead to higher land surface temperatures especially in densely populated urban cores thereby exacerbating UHI intensity.

Sixty eight percent (68%) of global populace is predicted to dwell in cities by 2050 (Affairs, 2019). Report from the United Nations indicates that the level of urbanization rose from 29% to 55% between 1950 and 2018 (Najafzadeh et al., 2021). It is anticipated that Africa will enter the "urban age" at a rate that has never been seen before (Güneralp et al., 2017). Africa may be the least urbanized continent in the world, but it is certainly becoming urbanized at one of the fastest rates. The population of Africans residing in cities has increased dramatically, from an estimated 28% in 1980 to 43% in 2018 and is anticipated to reach almost 60% by 2050 (Simwanda et al., 2019).

Over the past century, Ghana has witnessed extensive urbanization of its rural areas. Urban population proportions rose from 9.4% in 1931 to around 50.9% in 2010 (Ghana Statistical services, 2014), reflecting rapid urbanization trend. In the Bolgatanga municipality, 49.8% of the populace are dwelling in developed areas, relative to the national proportion of 50.9% and the regional 21% of urban population percentage (Korah et al., 2023). This development has led to extensive Land Use and Land Cover

Change (LULCC), primarily fueled by industrial growth, infrastructure development and its associated impermeable ground cover including concrete and asphalt. These elements are characterized by great thermal capability, disrupt natural energy balances and contribute to the intensification of UHI effect (Wemegah et al., 2020). There has been a surge in Kumasi's mean surface temperature by 1.2 °C over the last five decades, largely attributed to rapid urbanization and land cover transformations.

Urban heat islands studies has been conducted in several established cities across the globe, including Lódz, Poland, Athens, Glasgow, Japan, and Asian megacities (Islam et al., 2016). Studies on UHI effect in Ghana remain limited (Buo et al., 2021). Buo et al., (2021) notably studied the spatial expansion of developed regions and the accompanying surge in UHI effects in Accra and Kumasi between 2002 and 2017. Their findings reveal that urban sprawl, particularly transformation of vegetated and bare lands to built-up areas considerably elevate the earth's surface heat, with UHI magnitudes in the tropical areas including Ghana exceeding those recorded in European counterparts during heatwaves event.

Although projections suggest that Northern Ghana will undergo accelerated warming, with temperatures expected to increase by roughly 1.5 ˚C to 3 ˚C over the next fifty years (Klutse et al., 2020), empirical research on UHI dynamics in the region remains scarce. Bolgatanga, for instance, has recorded a warming rate of 0.024 ˚C, highlighting the vulnerability of semi-arid urban centers to climate-induced thermal stress. By concentrating mainly on southern cities including Accra and Kumasi, existing studies such as Wemegah et al., (2020) on UHI in Ghana have created a major knowledge gap in understanding spatiotemporal changes of land surface heat in northern towns (Peng et al., 2020). This gap poses public health concern, particularly given the areas urbanization, limited vegetation cover and heightened exposure to extreme temperature

The research adds to the expanding literature on urban by presenting the first comprehensive spatio-temporal analysis of UHI dynamics in Bolgatanga municipality, Ghana, an area notably underrepresented in existing literature. Through the integration of multitemporal Landsat imagery, meteorological datasets, and advanced thermal modeling, the research establishes a replicable framework for quantifying urban thermal anomalies in semi-arid cities with limited data availability. The findings reveal

significant thermal intensification driven by land use changes, notably the spread of non-permeable surfaces and the reduction of plant cover.

These results are crucial not only for guiding climate resilient urban planning in Bolgatanga but also for informing strategies in other rapidly urbanizing regions across sub–Saharan Africa and the global south that share similar climatic and developmental contexts. By addressing both geographical and methodological gaps, the study advances the discourse on urban thermal vulnerability in data scarce environment.

2. Materials and methods

2.1 Study area

The study domain is the Bolgatanga Municipality, located in Ghana Upper East Region. Covering an area of approximately 729km^2, the municipality lies amid latitudes 10˚30′N and 1˚55′N and 0˚33′W and 1˚00′W. It shares boundaries with the Talensi and Nabdam Districts to the south, and east respectively, Bongo to the North, and Kassena Nankana West district to the west (Fig. 1).

Bolgatanga experiences a Sudanese type of climate, marked by distinct wet and dry seasons. Rainfall follows a unimodal pattern, typically occurring between April and September, with an annual average of about 1150mm (Braimah et al., 2014). Peak temperatures often exceed 40° C, particularly in March and April. The natural vegetation is dominated by savannah woodland, consisting of drought resistant deciduous trees interspersed with perennial grasses

Demographically, the municipality has undergone rapid urbanization. The 2010 population and housing census reported 131,550 residents, of whom 65,512 (49.8%) lived in urban areas. A decade later, the Ghana statistical services (GSS, 2021) recorded an increase to 139,864 residents, with 89,253 (63.8%) in urban settlements and 5,609 (36.2%) in rural areas. These significant demographic shifts underscore the need to examine the UHI effect within the municipality, given the growing urban footprint and its potential implications for thermal stress

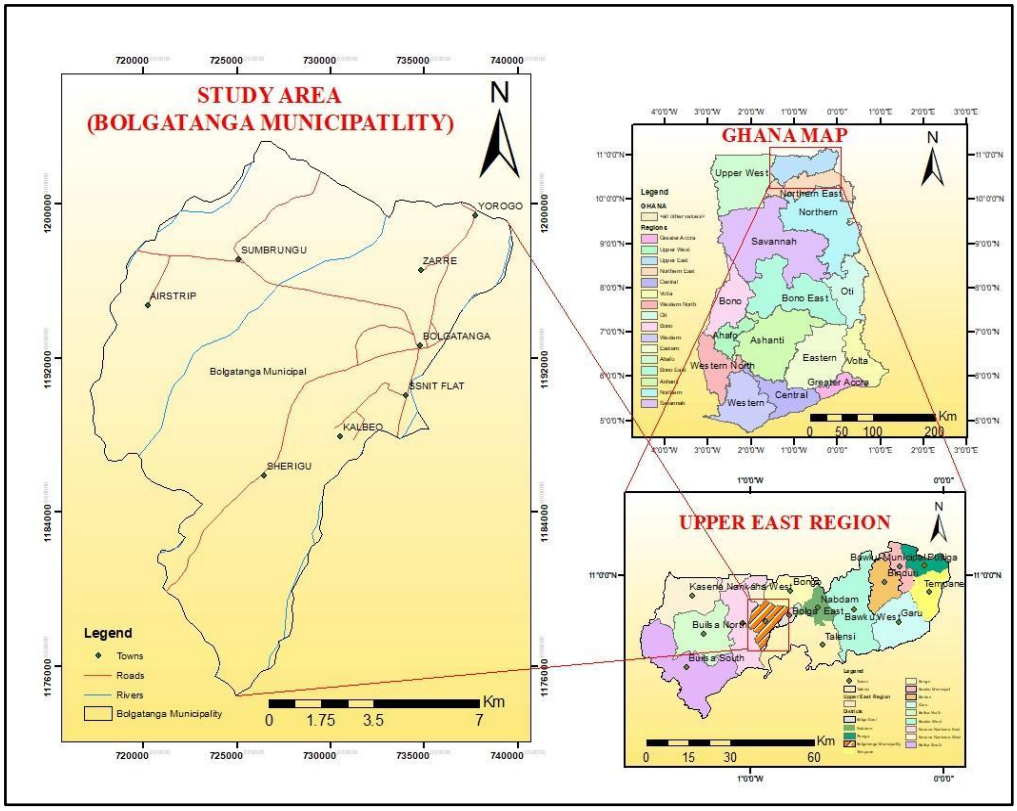


Fig.1 The study area (Bolgatanga Municipality) in Ghana

2.2 Description of the dataset

To assess the spatiotemporal dynamics of UHIs in Bolgatanga municipality, satellite and meteorological datasets for the years 2007, 2014 and 2021.

2.2.1 Remote sensing data

Landsat 5 Thematic Mapper and Landsat 8 Operational Lands Imager (OLI) collection 2 level 1 data were downloaded from the USGS earth explore website (http://glovis.usgs.gov). The selected scenes correspond to Path 194 and Row 053, covering the study area. Table 1 summarizes the sensor category and acquisition details.

Table 1: Landsat Sensor type and image acquisition date

Sensor Type	Acquisition date	Acquisition time
LandSat5 TM	11th April 2007	10:15:29
LandSat8	29th March 2014	10:20:55
LandSat8	12th February 2021	10:20:46

2.2.2 Meteorological data

Ancillary meteorological parameters, including air temperature, wind speed, and relative humidity, were retrieved from the NASA Power Access viewer (https://power.larc.nasa.gov/data-access-viewer/). These datasets, spanning over four decades of solar-based observations, were selected to match the acquisition dates of the Landsat imagery. Table 2 presents the meteorological conditions corresponding to each satellite image date.

Table 2: Meteorological datasets (air temperature, windspeed and relative humidity) used for the study

Date	**Minimum Air Temperature(°C)**	**Maximum Air Temperature(°C)**	**Windspeed (Km/h)**	**Relative Humidity (%)**
11th April 2007	24	31.78	7	0.41
29th March 2014	25	37.76	5	0.21
12th February 2021	27	39.97	11	0.08

2.3 Land use mapping

The supervised classification approach was applied in the land cover mapping with a support vector Machine (SVM) algorithm to establish spatial association between UHI patterns and land cover types, following the approach of Islam et al., (2016). Four primary land cover categories were delineated: vegetation, bare land, water, and built-up areas.

2.4 Estimating surface temperature

Using the Mono Window Algorithm (MWA), land surface temperature (LST) was derived from the thermal infrared bands of Landsat 5TM (Band 6) and Landsat 8 OLI/TIRS (Band 11). MWA integrates radiative transfer principles with atmospheric and surface parameters. The algorithm relies on three key inputs: atmospheric transmittance, land surface emissivity (LSE), and air temperature (Dos Santos et al., 2017). Fig. 2 and Fig. 3 illustrate the methods for obtaining the parameters how they are used in the mono window technique

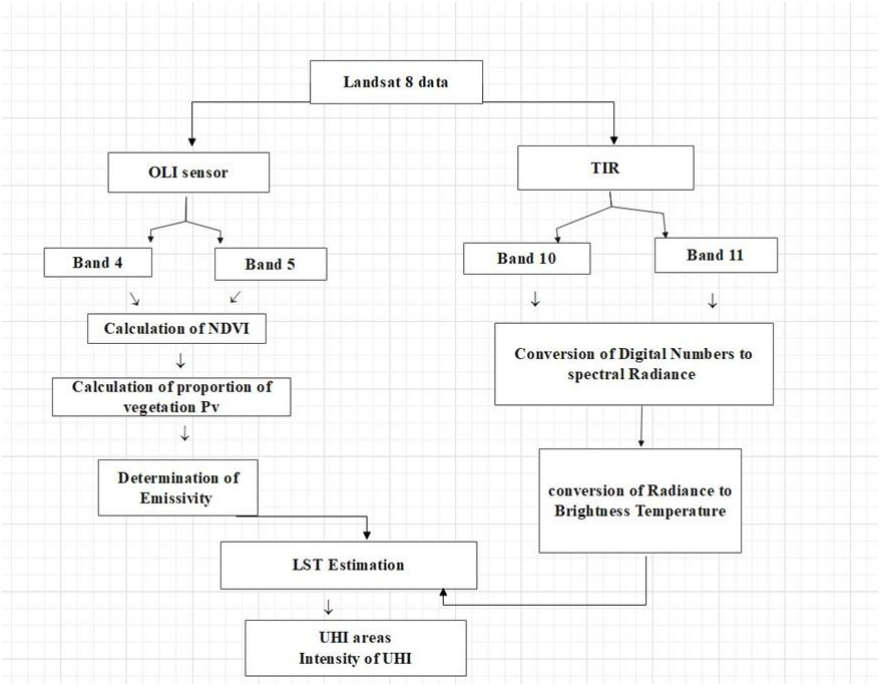


Fig. 2 Flow diagram of the approach used in deriving the Urban Heat Island Intensity (UHII) from Landsat 8 imagery

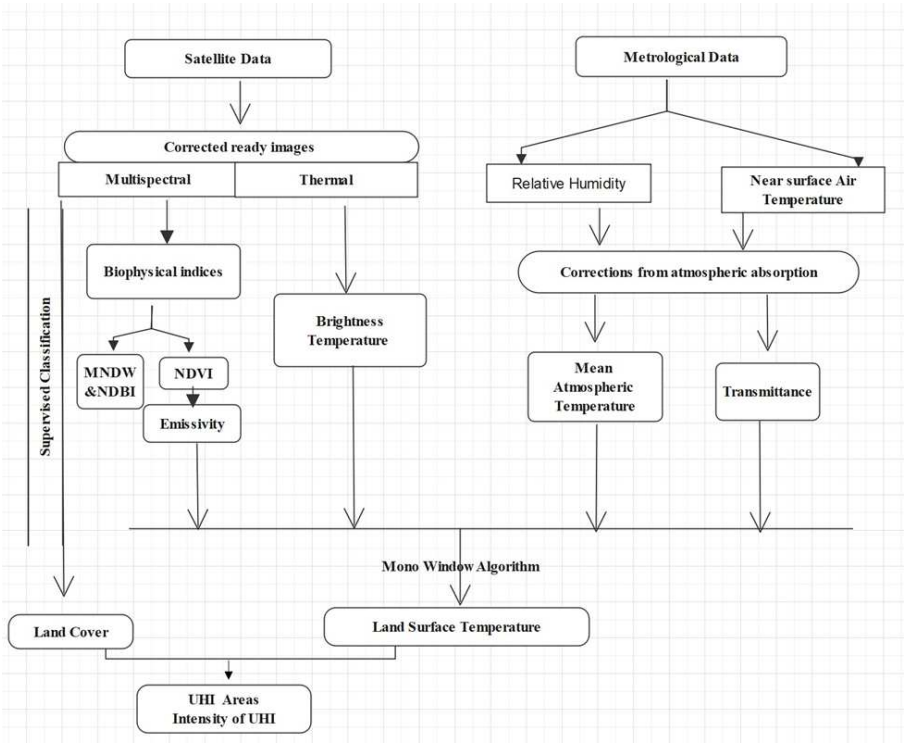


Fig. 3 Flowchart of the approach adopted in deriving the Urban Heat Island Intensity (UHII) Landsat 5 imagery

2.4.1 LST retrieval from Landsat 8

The six steps procedure for determining LST from Landsat-8 imagery (Dr. S. Varadanjan, (2021); Mirsanjari et al., (2021); (Sekertekin et al., 2016). is outlined below:

Step 1: Spectral radiance conversion

This involves conversion of raw digital numbers (DN) captured by satellite sensors into Top of Atmospheric Reflectance (meaningful radiance values). Computation is done with the band specific parameters provided in the image metadata file, using a simple linear equation. After conversion, the resulting L_λ represents the at- sensor spectral radiance measured in W/(m^2.sr.µm). The equation is as follows.

$$L_\lambda = M_L \times Q_{cal} + A_L - O_i \quad (1)$$

Where;

L_λ –Radiance per unit wavelength interval

M_L – Multiplicative rescaling factor for a specific Band

Q_{cal} - Quantized calibrated pixel value

A_L- Band specific additive rescaling factor

O_i - Adjustment factor

Step 2: Brightness temperature (BT)

Top of Artmosphere (TOA) radiance to brightness temperature using:

$$B_T = \frac{K_2}{In\left[\left(\frac{K_1}{L_\lambda}\right)+1\right]} - 273.15 \quad (2)$$

Where;

B_T - Brighteness Temperature in °Celsius,L_λ- Spectral radiance of TOA $\left(\frac{mW}{sr\ mm^2}\right)$,

M_L- Multiplicative rescaling value,Q_{cal} -Digital Number (As a calibrated and quantized pixel value),A_L - Band specific additive rescaling factor, O_i - Adjustment factor.K_1 and K_2 - Band specific thermal conversions constants, L_λ - TOR spectral radiance (Band 10)

Step 3*:* Vegetation Index computation

Normalized Diference Vegetation Index (NDVI) was computed using bands 4-0.64 μm (Red reflectance) and 5-0.85 μm (NIR reflectance):

$$NDVI = \frac{(Band5 - Band4)}{(Band5 + Band4)} \quad (3)$$

NDVI values vary from -1 to +1 and were subsequently use dt estimate vegetation fraction and emissivity.

Step 4: Vegetation proportion (Pv). Vegetation proportion was derived from NDVI raster:

$$P_V = \left(\frac{NDVI - NDVI_{min}}{NDVI_{max} - NDVI_{min}}\right)^2 \quad (4)$$

Step 5 Surface Emissivity Determination

Land surface emissions were estimated using the NDVI threshold approach. In this approach emissivity is derived from the NDVI by assigning higher values (0.98 - 0.9) to dense vegetation and lower values (0.95 - 0.97) to bare land using the linear equation:

$$\varepsilon = \varepsilon_S\,(1 - P_V) + \varepsilon_V P_V + d\varepsilon \quad (5)$$

Where;

ε_V -Emissivity of vegetation

ε_S – Emissivity of soil

P_V – Fractional vegetation cover

For Landsat 8 the final emissivity was refined as:

$$\varepsilon = 0.986 + 0.004 \times P_V$$

0.004 – Standard deviation in soil emissivity across thermal bands

0.989 – Mean vegetation and soil emissivity factors

Step 6: Final LST Estimation

The LST was estimated from the Top of Atmospheric Brightens Temperature by applying an emissivity correction using the radiative transfer formula:

$$LST = \frac{BT}{\{1+\left[\left(\frac{\lambda BT}{\rho}\right)In(\varepsilon\lambda)\right]\}}{}^{0}C \quad (7)$$

Where;

$\lambda - 10.8\mu m$ (wavelength of emitted radiance)

$\varepsilon\lambda$ –surface emissivity

$$\rho = h\frac{c}{\sigma} = 14388\mu m\ K$$

Where;

$c -$ Velocity of light (3x10^8m/s

σ – Boltzmann's (138 $\times 10^{-25}$ J/K) and

2.4.2 Landsat 5 TM specific calibration

Step 1 Radiance correction

For Landsat 5 TM, radiance correction was applied using:

$$L_\lambda = L_{min} + \frac{(Lmax-Lmin)}{(Qcalmax-Qcalmin)}(QcalDN - Qcalmin) \quad (8)$$

Where;

L_λ – Electromagnetic radiation reaching the sensors aperture $\left[\frac{W}{(m^2.Sr.\mu m)}\right]$

$Lmin\lambda$ – at - sensor spectral radiance corresponding to Q_{calmin} $\left[\frac{W}{(m^2.Sr.\mu m)}\right]$,

$Lmax\lambda$ - at - sensor spectral radiance corresponding to Q_{calmax} $\left[\frac{W}{(m^2.Sr.\mu m)}\right]$,

QcalDN-integer assigned to each pixel a given spectral band

$Qcalmin$ – lower bound of the quantized calibrated DN (corresponding to $LMIN_\lambda$, for Landsat)

$Qcalmax$- upper bound of the quantized calibrated DN (corresponding to $LMAX_{\lambda, \text{ for}}$ Landsat TM =255)

Brightness temperature was then derived as:

$$T_b = \frac{K_2}{In\left(\frac{K_1}{L_\lambda}\right)+1} \quad (9)$$

Where; T_b is the brightness temperature, and (^{0}K), K_1 and K_2 are the Band dependent thermal coefficient with K_1 and K_2 for TM5 being 607 and 1260.56 respectively (Sekertekin et al., 2016).

Step 2: Atmospheric transmittance and mean air temperature

The mono-window algorithm requires radiometric calibration to correct for the absorption and attenuation of thermal radiation by water vapor content. This method allows for effective correction of atmospheric effects without depending on ground truth data, making the Mono window algorithm more practical for local and regional LST retrieval. The atmospheric vapor content (W) was estimated using surface air temperature (T_0) and relative humidity (RH) following the formulation by Dos Santos et al., (2017) and Islam et al., (2016):

$$W = 0.0981 \times \{10 \times 0.6108 \times exp\left[\frac{17.27 \times (T0-273.15)}{(237.3+(T0-273.15)}\right] RH\} + 0.1697 \quad (10)$$

Where;

W - The atmospheric vapor content (g cm^{-2}),

T0 – Near surface air temperature (K), and

RH – the relative humidity (%).

The atmospheric transmittance (T_i) was then calculated as Dos Santos et al. (2017)

$$T_i = 1.031412 - 0.11536 \times W \quad (11)$$

Where: Ti - atmospheric transmittance, and W - water vapor content

Step3: Land Surface Emissivity

Surface emissivity was computed by means of the NDVI threshold approach as described in Islam et al., (2016). The same emissivity estimation equation (equations 4,5) used for Landsat 8 data were applied to Landsat 5 raster data to ensure consistency across sensors.

Step 4: Effective atmospheric temperature

The effective atmospheric temperature also known as the mean atmospheric temperature is the average temperature of the entire air column above the ground. It is weighted in a way that reflects how much each layer contributes to the thermal radiation detected by the satellite. This was determined by the empirical relationship proposed by (Bektaş Balçik, 2014):

$$T_a = 16.0110 + 0.92621 \times T_0 \quad (12)$$

Where;

T_a – Average atmospheric temperature,

T_0 – Surface air temperature (Kelvin).

Step 5: LST retrieval from Landsat 5TM

The final LST using the MWA was estimated by combining the sensors atmospheric transmittance with the correction for land surface emissivity and atmospheric temperature (Bektaş Balçik, 2014):

$$T_S = \frac{\{a \times (1-C-D) + [b \times (1-C-D) + C + D] \times T_b - D \times T_a\}}{C} \quad (13)$$

Where;

T_S – is LST 9 (Kelvin),

T_b – is brightness temperature (Kelvin), constants a=−67.355351 and b=0.458606 are empirical coefficients specific to landsat 5, Ta represents the mean atmospheric temperature, C and D are midway transmittance factors;

$$C = \varepsilon_i \times T_i$$

$$D = (1 - T_i) \times [1 + (1 - \varepsilon_i) \times T_i]$$

Where;

ε_i- is emissivity

2.5 Urban heat islands intensity index (UHII)

UHI patterns were analyzed using the UHI index, which quantifies the temperature gradient distinguishing developed and less developed regions (Sultana and Satyanarayana,2020):

$$T_r = \frac{T_i - T_a}{T_a}$$

Where;

T_r - How much cooler or warmer a location is relative to the study area average (Relative LST).

T_i - Site-specific LST

T_a - Study area's mean LST

2.5.1 Normalized Difference Built- up index (NDBI) estimation

Built-up areas were identified using the NDBI, which exploits the higher reflectance of developed surfaces in the MIR relative to the NIR wavelength range (Bektaş Balçik, 2014; Islam et al., 2016).

$$NDBI = \frac{MIR - NIR}{MIR + NIR}$$

where MIR and NIR represent the Landsat data's medium infrared and near-infrared bands, respectively.

2.5.2 Modified Normalized Difference Water Index (MNDWI) estimation

The MNDWI was applied to effectively delineate water bodies in the study area. This index uses the pronounced difference in reflectance between the green band and the mid-infrared band, where water bodies typically show high reflectance in the green band and strong absorption in the MIR band (Bektaş Balçik, 2014; Islam et al., 2016).

$$MNDWI = \frac{G - MIR}{G + MIR}$$

Where G is a green band of the Landsat data.

2.5.2 UHII stack profiling

UHII stack profile was conducted to analyze the spatial variability of surface heat intensity across various land cover classes within the Bolgatanga municipality. The analysis involved segmenting UHII maps for the study years (2007, 2014 and 2021) in ArcGIS to quantify both the strength and geographical spread of the UHI effect across urban, newly developed, and rural areas. By overlaying UHI layers with classified LULC maps, variations in surface temperature intensity were systematically profiled for each land cover category. This approach enabled the identification of temporal shifts in heat concentration and delivered an in-depth assessment of how expansion of urban areas and decline of plant cover influenced the intensity and spatial distribution of UHIs over time.

3.0 Results

3.1 Land cover dynamics

Supervised classification of Landsat data highlighted notable shifts in land cover patterns in Bolgatanga Municipality between 2007 and 2021. Fig.4 and 5 illustrate the variations in the areal coverage of each land use type over the study period and associated change statistics. Built-up areas surged from 96.36 km^2 in 2007 to 137.64 km^2 in 2021, an increase of 43%. Bare soil also rose from 120.99 km^2 to 137.64 1 km^2, while vegetation cover declined sharply by 56%, from 107.25 km^2 to 46.71 km^2. Water bodies showed a marginal reduction from 0.76 km^2 to 0.24 km^2 as indicated in Fig.5(d). (d).

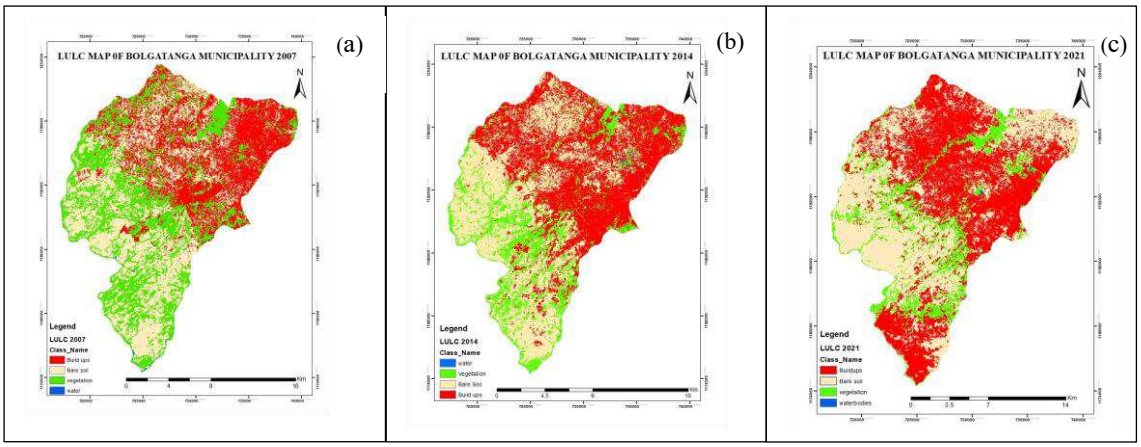


Fig. 4 Land use and Land cover (LULC) classes in Bolgatanga municipalities for 2007(a), 2014(b), and 2021(c)

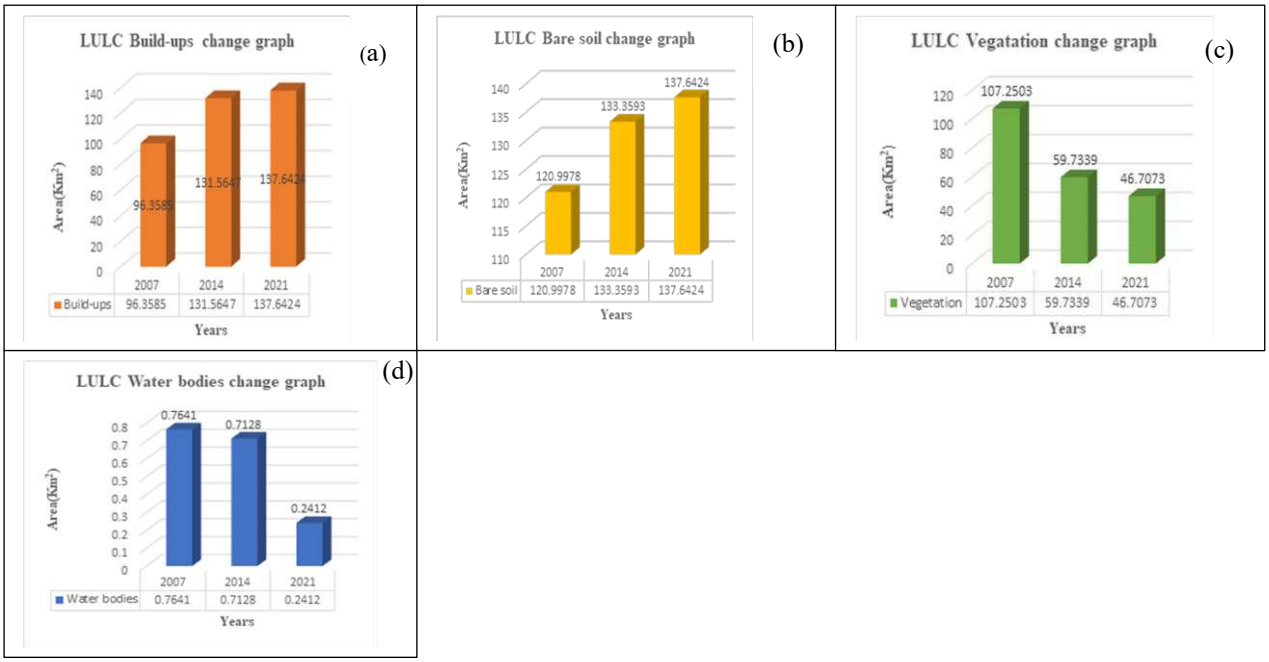


Fig. 5 Extent of built-up(a), bare soil(b), vegetation(c) and water bodies(d) in Bolgatanga Municipal over the years 2007, 2014 and 2021

These changes reflect rapid urban expansion and land degradation, particularly in peri-urban zones such as Sumbrungu, where poor planning and deforestation have intensified land surface modification.

3.2 Trends of Land surface temperature (LST)

LST analysis indicated a persistent trend throughout the municipality. The average LST rose from 27.94˚ C in 2007 to a peak of 35.39˚C in 2014, before marginally decreasing to 34.81 ˚C in 2021. However, maximum LST rose steadily, reaching 42.46˚C in 2021 thus a 26% increase from 2007, as shown

in Fig. 6. This suggests intensifying heat stress, particularly in densely built-up and bare soil zones.

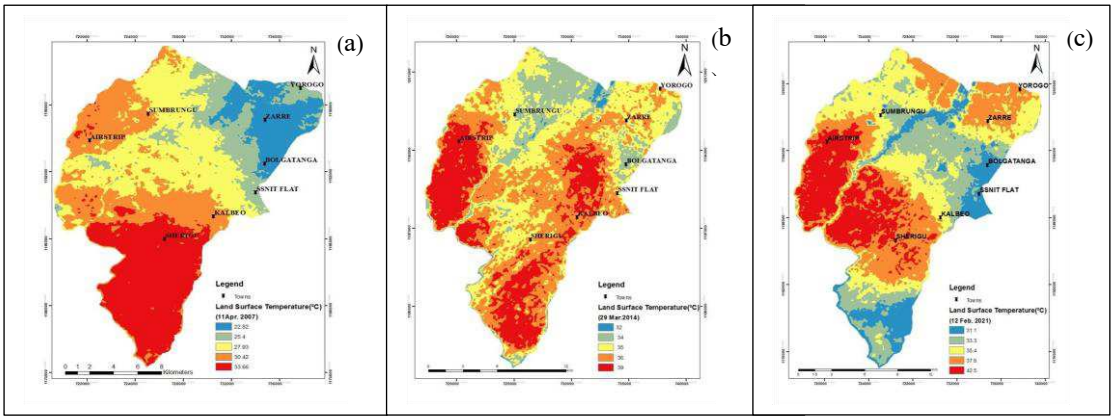


Fig. 6 Spatiotemporal trends in LST dynamics in Bolgatanga municipal for 2007(a), 2014(b), and 2021(c)

Spatial LST maps (Fig. 5) show that high-temperature zones expanded outward from the urban core into newly developed areas. Vegetated and water-covered zones consistently exhibited lower LST values, reinforcing their cooling role. The temporal trend of mean and maximum LST is visualized in Fig. 6.

3.3 Validation with Meteorological Data

To ensure accuracy, table-driven LST values were validated against NASA POWER meteorological datasets. The 2007 dataset demonstrated near perfect agreement, with a variance of 0.0013. In contrast, the 2014 and 2021 datasets showed larger discrepancies, with variance of 8.04 and 1.07, respectively. These differences are likely attributable to spatial heterogeneity and the inherent limitations of point-based ground measurement in capturing the complex gradients present across urban environments. The comparative results are presented in Table 3.

Table 3: Contrast between mean LST from satellite data and ground station measurement

Date	Mean of LST (°C)	Mean of meteorological Temperature (°C)	Variance	Standard Deviation
11th April, 2007	27.94	27.89	0.0013	0.0354

29thMarch,2014	35.39	31.38	8.0401	2.8355
12thFebruary,2021	34.81	33.35	1.0658	1.0324

According to Rongali et al., (2018) satellite driven LST values compared with meteorological ground data may exhibit an error margin of up to 5°C, with accuracy in some cases reaching ±2°C when validation against actual ground temperature measurements.

3.4 Urban Heat Island Intensity Index

The UHII maps (Fig 7 a, b, and c) reveal a clear intensification of thermal anomalies over time. The highest UHII values recorded were 1.7 ˚C in 2007, 2.76 ˚C in 2014, and 2. 69 ˚C in 2021. The spatial distribution indicates that newly developed rural areas are increasingly affected, largely due to land cover transitions and declining vegetation. Built-up areas consistently recorded the greatest UHII values, whereas water bodies and vegetated covers remained relatively thermally stable throughout the study period.

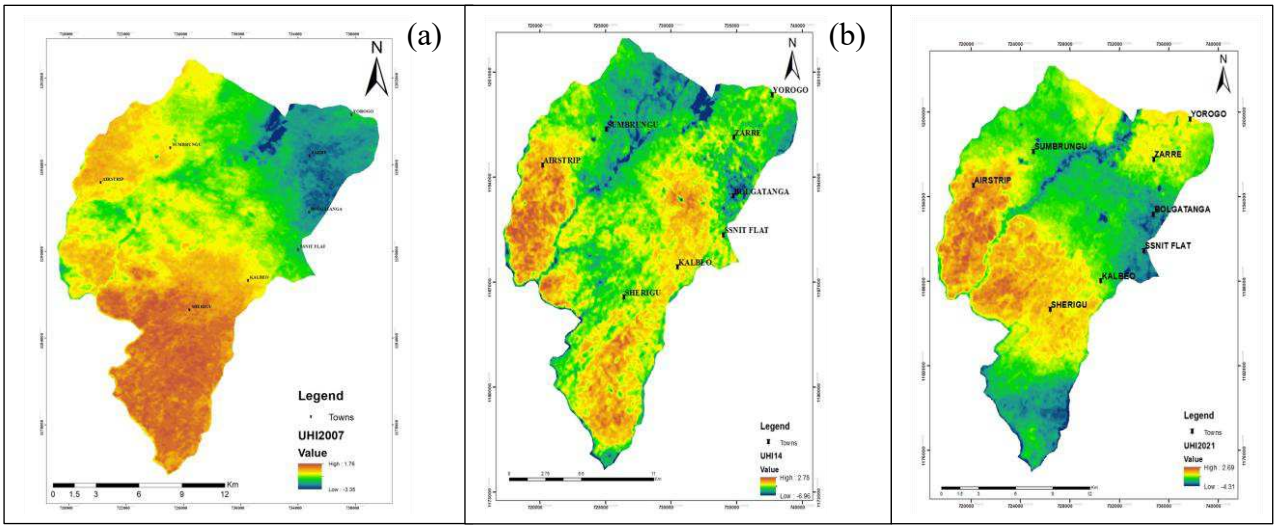


Fig. 7 Urban Heat Island Intensity (UHII) in Bolgatanga municipalities for 2007(a), 2014(b) and 2021(c)

3.5 UHII stack profiling

Stack profiling across urban, peri urban and rural areas (Fig 8) revealed distinct thermal gradients. In 2007, UHII was largely concentrated within the urban core. By 2014 and

2021, elevated UHII values had expanded into newly developed areas such as Sumbrungu, reflecting the influence of urban sprawl and the widening thermal footprint.

The profiles further indicate that rural areas, which were previously thermally neutral, now exhibit UHII values approaching those of urban areas. This shift underscores the loss of ecological buffers and highlights the growing vulnerability of rural landscapes to heat stress.



Fig. 8 Urban Heat Island Intensity (UHII) profile across urban, newly developed and rural areas in Bolgatanga municipality

3.6 Land Cover- Temperature Correlation

To analyze the effect of vegetation on surface temperature, a correlation assessment was performed between UHII, NDBI and NDVI. Ten pixels values were randomly sampled from the LST raster and matched with corresponding NDBI and NDVI values across the study area. Findings revealed a strong coefficient of determination (r^2) which ranges between 0.79 - 0.9 over the years of study. This confirms that vegetation areas consistently exhibit lower surface temperatures. The significant positive correlation among LST and NDBI, with r^2 values fluctuating from 0.51 to 0.83, suggests that urban and impervious surfaces substantially contribute to elevated thermal intensity. Fig. 9, 10 and 11 presents the correlational plots.

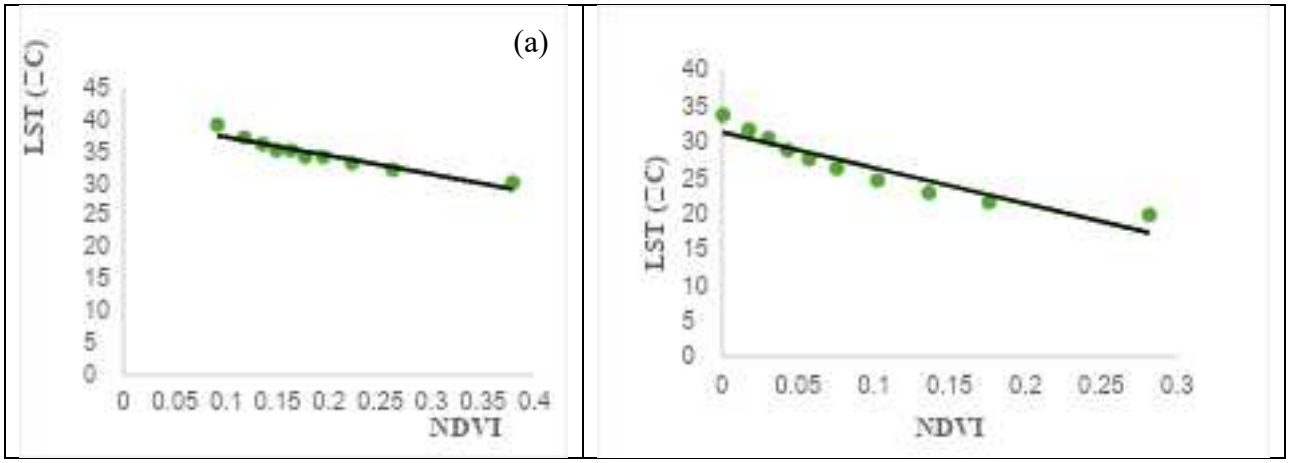


Fig. 9 Correlation between LST and NDVI for March,2007 (a) and April,2014(b)

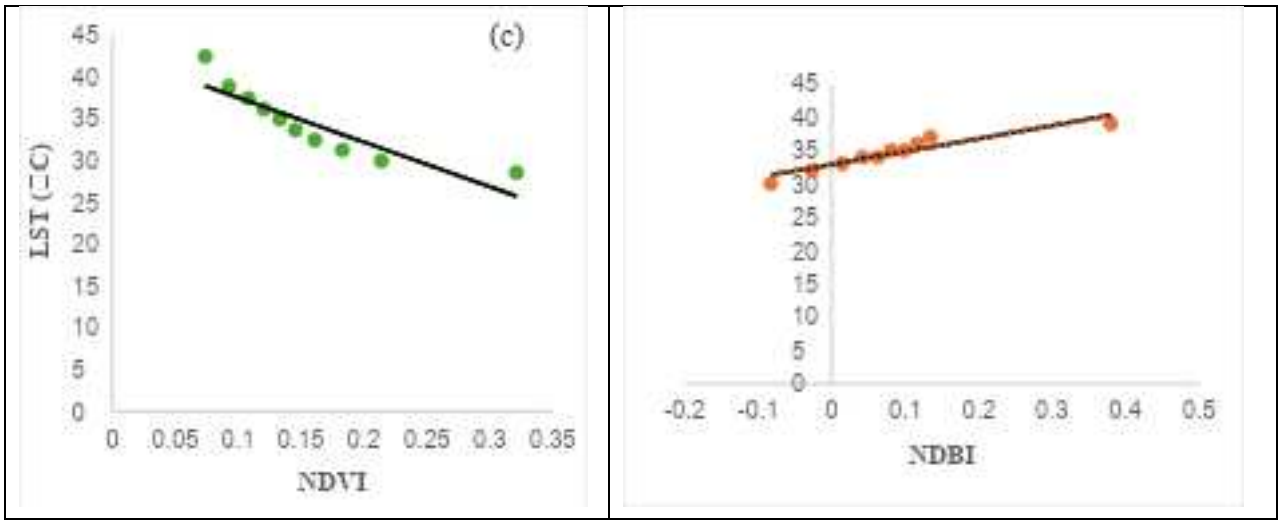


Fig.10 Correlation between LST and NDVI(c) for February, 2021 and LST and NDBI(d) for February 2007

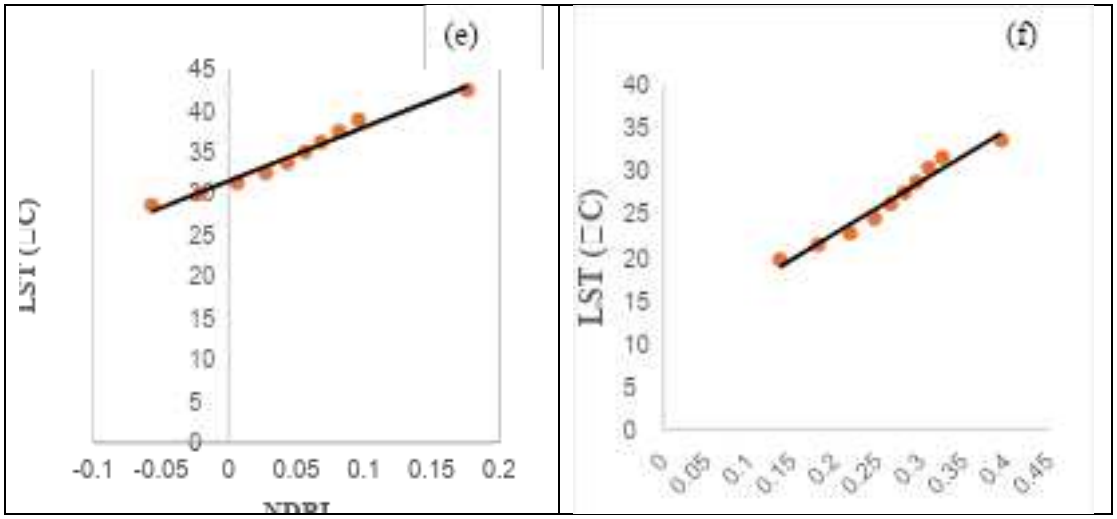


Fig. 11 Correlation between LST and NDBI for March, 2014(e) and February 2021(f)

4.0 Discussion

This study utilized multitemporal Landsat imagery alongside meteorological datasets to analyze the spatial and temporal patterns of UHIs in Bolgatanga municipality, Ghana. The outcome reveals a notable rise in land surface temperature (LST) and UHI effects over the 14-year timeframe, driven primarily by rapid urban expansion, vegetation losses, and land cover transformation. These findings carry critical repercussions for climate resilience, city planning, and population wellbeing in Northern Ghana.

4.1 Land cover dynamics and drivers of urban thermal intensification

Spatial analysis revealed that built up areas expanded by more than 40% between 2007 and 2021, while vegetated land declined by over 56%. This transition coincided with an increase in average LST from 27.94 ˚C to 34.8 ˚C and a peak UHII of 2.76 ˚C in 2014. The growth of impermeable areas and the decline of evapotranspirative cover altered the surface energy balance, intensifying heat retention and diminishing nighttime cooling.

Comparable studies in West African cities such as Accra, Ouagadougou, and Bamako (Buo et al.,2021; Simwanda et al., 2023; Assaf et al., 2023), have reported similar thermal escalations linked to impervious surface expansion and vegetation decline. However, Bolgatanga's semiarid climate and limited vegetative buffers make it uniquely vulnerable to heat stress, with fewer ecological mechanisms available to mitigate thermal anomalies.

Furthermore, UHII profiling across urban, pre-urban, and rural areas shows that thermal stress is no longer confined to city cores but has spread into newly developed and rural areas, reflecting a widening heat footprint. This suggests that mitigation strategies must extend beyond central districts to include transitional and rural urban fringes. Similar patterns have been observed in Ouagadougou, Burkina Faso (Zong et al., 2022), and Kano, Nigeria (Abdullahi et al., 2020), where urban sprawl has intensified surface heat exposure in peripheral zones.

Plant cover serves a vital function in regulating urban microclimates via shading and evapotranspiration. In Bolgatanga, vegetated cover declined from 107.25km^2 to

46.71km^2, a change accompanied by a 14.52 ˚C increase in maximum LST. Spatial LST maps and UHII profiles consistently show lower temperatures in vegetated and water covered areas, reinforcing their role as thermal refuges. This trend aligns with discoveries by Simwanda et al. (2023), who demonstrated that NDVI values inversely correlate with LST in rapidly urbanizing African cities. The loss of vegetative buffers raises concerns about long-term climate resilience, particularly given the municipality's susceptibility to extreme heat and drought.

Correlation analysis between LST, NDVI, and NDBI provides quantitative evidence of land cover influence on surface temperature. A strong inverse association was observed between LST and NDVI (r^2= 0.79- 0.90), confirming that greater plant cover corresponds to lesser surface temperatures. Conversely, a significant positive relationship was identified among LST and NDBI (r^2= 0.51- 0.83), indicating that built-up areas substantially contribute to thermal intensification. These relationships validate the use of sectoral indices as proxies for thermal behavior and support the integration of remote sensing into urban heat monitoring frameworks (El-Magd et al., 2016; Sultana & Satyanarayana, 2019; Islam et al., 2016)). The consistency of these trends across all study years highlights the robustness of spectral indices in characterizing urban thermal dynamics.

4.2 Integrating climate adaptation into municipal planning

The intensification of UHIs in Bolgatanga has direct implications for urban livability, energy demand, plant growth, concentration of air pollutants and public health (Najafzadeh et al., 2021). The recorded 56% drop in land cover and the extension of thermal hotspots towards peri-urban areas underscore the necessity of weaving climate adaptive designs into municipal governance. Without climate-sensitive planning, the municipality risks exacerbating heat-related morbidity, especially among vulnerable populations. The findings signals the need for adaptive strategies such as:

1. Preservation and expansion of vegetated zones and green corridors
2. Promotion of permeable surfaces and reflective roofing materials
3. Integration of UHI metrics into zoning and land use policies. zoning regulations that limit impervious surface proliferation could serve as low-cost, high-impact adaptation strategies.

4. Deployment of urban forestry, afforestation and water-sensitive design principles

Recent work by Assaf et al. (2023) advocates for embedding remote sensing into urban planning frameworks to guide heat mitigation efforts. This study reinforces that recommendation, demonstrating the utility of Landsat-derived LST and UHII metrics in identifying thermal hotspots and informing targeted interventions.

4.3 Methodological Strengths and Limitations of the study

The application of Mono - Window Algorithm (MWA) for LST retrieval, combined with synchronized meteorological datasets, enabled high - resolution thermal assessment across heterogeneous landscapes. The strong alignment between satellite driven and ground-based temperatures in 2007 validates the robustness of this approach. However, discrepancies observed in subsequent years highlight the need for more granular ground observation and improved calibration of atmospheric parameters.

While the study provides valuable spatial insights, its temporal resolution is restricted to three discrete years. Future research could benefit from incorporating higher frequency dataset (eg., MODIS, Sentinel 3) and applying machine learning models to enhance predictive UHI mapping and develop early warning systems.

5.0 Conclusion and Recommendations

5.1 Conclusion

This study employed multitemporal Landsat imagery and meteorological data to examine the spatiotemporal patterns of urban heat islands in Bolgatanga municipality, Ghana. The findings show a profound rise in land surface temperature (LST) and UHII effects from 2007 to 2021, driven by rapid urban sprawl, Deforestation, and land cover transformation.

Key findings include:

- Built up areas increase by 43% while plant cover declined by 56% between 2007 and 2021
- A rise in average LST from 27.94 ˚C to 34. 81˚C, with maximum LST reaching 42.46 ˚C in 2021.

- Peak UHI Values of 2.76 ˚C, with thermal stress extending into newly developed and rural areas.
- A significant inverse relationship was observed between LST and NDVI (r^2= 0.79- 0.90), and a strong positive correlation was identified among LST and NDBI (r^2= 0.51- 0.83), confirming the temperature moderation function of plant cover and the heat enhancing impact of urban structures.

These results highlight the urgent need for climate resilient planning in Northern Ghana's urban areas, where rising temperatures and rapid urbanization pose serious risks to environmental sustainability and public health

5.2 Recommendations

These recommendations are proposed based on the study findings**:**

1. **Integrate UHI metrics into urban planning:** Local governments and planners should incorporate satellite derived LST and UHII metrics into zoning and development decisions. This study demonstrates the utility of such data in identifying thermal hotspots, offering a replicable framework for managing urban thermal risks in Bolgatanga and other northern municipalities.
2. **Preserve and expand vegetation cover:** Urban greening initiatives including tree planting, green corridors, and rooftop gardens should be prioritized to mitigate heat stress and enhance microclimatic regulations.
3. **Promote responsive climate infrastructure:** Encourage the adoption of reflective roofing materials, permeable pavements, and heat resilient building designs to reduce surface heat absorption and improve thermal comfort.
4. **Strengthening policy and institutional capacity:** Develop and enforce land use policies that curb unregulated expansion and incentivize sustainable development practices, particularly in pere-urban and ecologically sensitive zones
5. **Support further research and capacity building:** Promote interdisciplinary research on urban climate dynamics and invest in training programs for municipal planners, GIS analysis, and environmental scientists to enhance local expertise and capacity

By implementing these measures, Bolgatanga municipalities across west Africa can strengthen resilience against urban heat risks while fostering sustainable, climate adaptive urban development.

Declarations

Funding

This research received no specific grant from any funding agency in the public, commercial or non- profit sector

Clinical trial

Clinical trial number: not applicable

Trial Registration

Not Applicable

Consent to publish

Consent to publish declaration: Not Applicable

Data Availability

The dataset generated during and or/ analysed during the current study are available from the corresponding author on reasonable request.

Ethics Approval and consent to participate

Ethics approval and consent to participate declaration: Not Applicable

Author Contribution statement

Bumbas Azeez contributed to conceptualization, methodology, data curation, formal analysis and writing of the original draft. Joan A. Atulley: contributed to validation, and manuscript review and editing. Ramson Kabenla contributed to vvisualization and manuscript editing, and Steve Ampofo contributed to supervision, data interpretation and manuscript review. All Authors read and approved the final manuscript.

Competing interests

The authors declare that they have no competing interest

5.0 References

Abdelal, Q., Assaf, M. N., Al-Rawabdeh, A., Arabasi, S., & Rawashdeh, N. A. (2022). Assessment of Sentinel-2 and Landsat-8 OLI for small-scale inland water quality modeling and monitoring based on handheld hyperspectral ground truthing. *Journal of Sensors*, *2022*(1), 4643924.

Addas, A., Goldblatt, R., & Rubinyi, S. (2020). Utilizing remotely sensed observations to estimate the urban heat Island effect at a local scale: Case study of a University campus. *Land*, *9*(6), 191.

Affairs, U. (2019). *Introduction and policy implications* (pp. 1–8). Un. https://doi.org/10.18356/82f7ef6b-en

Bektaş Balçik, F. (2014). Determining the impact of urban components on land surface temperature of Istanbul by using remote sensing indices. *Environmental monitoring and assessment*, *186*(2), 859-872.

Braimah, M. M., Abdul-Rahaman, I., Oppong-Sekyere, D., Momori, P. H., Abdul-Mohammed, A., & Dordah, G. A. (2014). A study into the causes of floods and its socio-economic effects on the people of Sawaba in the Bolgatanga Municipality, Upper East, Ghana.

Buo, I., Sagris, V., Burdun, I., & Uuemaa, E. (2021). Estimating the expansion of urban areas and urban heat islands (UHI) in Ghana: a case study. *Natural Hazards*, *105*(2), 1299-1321.

Buyantuyev, A., & Wu, J. (2010). Urban heat islands and landscape heterogeneity: linking spatiotemporal variations in surface temperatures to land-cover and socioeconomic patterns. *Landscape ecology*, *25*(1), 17-33.

Dos Santos, A. R., de Oliveira, F. S., da Silva, A. G., Gleriani, J. M., Gonçalves, W., Moreira, G. L., ... & Mota, P. H. S. (2017). Spatial and temporal distribution of urban heat islands. *Science of the Total Environment*, *605*, 946-956.

Abou El-Magd, I., Ismail, A., & Zanaty, N. (2016). Spatial variability of urban heat islands in Cairo City, Egypt using time series of Landsat Satellite images. *International Journal of Advanced Remote Sensing and GIS*, *5*(3), 1618-1638.

Abou El-Magd, I., Ismail, A., & Zanaty, N. (2016). Spatial variability of urban heat islands in Cairo City, Egypt using time series of Landsat Satellite images. *International Journal of Advanced Remote Sensing and GIS*, *5*(3), 1618-1638.

Ghana Statistical Services (2014). 2010 population and housing census report on urbanization. *Ghana Statistical Service*, retrieved on October 25, 2025, from https://statsghana.gov.gh/gssmain/fileUpload/pressrelease/2010_PHC_National_Analytical_Report.pdf

Güneralp, B., Lwasa, S., Masundire, H., Parnell, S., & Seto, K. C. (2017). Urbanization in Africa: challenges and opportunities for conservation. *Environmental research letters*, *13*(1), 015002.

Gui, X., Wang, L., Yao, R., Yu, D., & Li, C. A. (2019). Investigating the urbanization process and its impact on vegetation change and urban heat island in Wuhan, China. *Environmental Science and Pollution Research*, *26*(30), 30808-30825.

Klutse, N. A. B., Owusu, K., & Boafo, Y. A. (2020). Projected temperature increases over northern Ghana. *SN Applied Sciences*, *2*(8), 1339.

Korah, P. I., Jambadu, L., & Nunbogu, A. M. (2023). Mapping spatial and temporal dynamics in urban growth: The case of secondary cities in northern Ghana. *Journal of Urban Affairs*, *45*(3), 390-406.

Lindén, J. (2009). Nocturnal cool island and a thermal wind-systemtwo features of the local climate in Ouagadougou, Burkina Faso. In *The seventh International Conference on Urban Climate. Yokohama, Japan*.

Liu, L., & Zhang, Y. (2011). Urban heat island analysis using the Landsat TM data and ASTER data: A case study in Hong Kong. *Remote sensing*, *3*(7), 1535-1552.

Mirsanjari, M. M., Mohammadyari, F., Visockiene, J. S., & Zarandian, A. (2021). Relationship between land surface temperature and urbanization in Vilnius district. *Environmental monitoring and assessment*, *193*(8), 472.

Mohammed, S. Y., Tanko, I. A., & Tayo Iyanda, Y. (2017). Urbanisation Effect on the Occurrence of Urban Heat Island over Kano Metropolis, Nigeria.

Nuruzzaman, M. (2015). Urban heat island: causes, effects and mitigation measures-a review. *International Journal of Environmental Monitoring and Analysis*, *3*(2), 67-73.

Peng, S., Piao, S., Ciais, P., Friedlingstein, P., Ottle, C., Bréon, F. M., ... & Myneni, R. B. (2012). Surface urban heat island across 419 global big cities. *Environmental science & technology*, *46*(2), 696-703.

Sekertekin, A., Kutoglu, S. H., & Kaya, S. (2016). Evaluation of spatio-temporal variability in Land Surface Temperature: A case study of Zonguldak, Turkey. *Environmental monitoring and assessment*, *188*(1), 30.

Simwanda, M., Ranagalage, M., Estoque, R. C., & Murayama, Y. (2019). Spatial analysis of surface urban heat islands in four rapidly growing African cities. *Remote Sensing*, *11*(14), 1645.

Sultana, S., & Satyanarayana, A. N. V. (2020). Assessment of urbanisation and urban heat island intensities using landsat imageries during 2000–2018 over a sub-tropical Indian City. *Sustainable Cities and Society*, *52*, 101846.

Wemegah, C. S., Yamba, E. I., Aryee, J. N. A., Sam, F., & Amekudzi, L. K. (2020). Assessment of urban heat island warming in the Greater Accra region. *Scientific African*,8, e00426. https://doi.org/10.1016/j.sciaf.2020.e00426

Zhao, L., Fan, X., & Hong, T. (2025). Urban heat island effect: remote sensing monitoring and assessment—methods, applications, and future directions. *Atmosphere*, *16*(7), 791.